TITLE: Integrated assessment of diclofenac biotransformation, pharmacokinetics, and omics-based toxicity in a 3D human liver-immunocompetent co-culture system

Ujjal Sarkar, Kodihalli C. Ravindra, Emma Large, Carissa L. Young, Dinelia Rivera-Burgos, Jiajie Yu, Murat Cirit, David J. Hughes, John S. Wishnok, Douglas A. Lauffenburger, Linda G. Griffith, and Steven R. Tannenbaum

Authors Affiliation:

Department of Biological Engineering, Massachusetts Institute of Technology, 77 Massachusetts Avenue, Cambridge, MA 02139, USA: US, KCR, CLY, DRB, JY, MC, JSW, DAL, LGG, SRT.

Department of Chemistry, Massachusetts Institute of Technology, 77 Massachusetts Avenue, Cambridge, MA 02139, USA: SRT.

CN Bio Innovations Ltd, Biopark, Broadwater Road, Welwyn Garden City, Hertfordshire, AL7 3AX, UK: EL, DJH.

RUNNING TITTLE: Diclofenac metabolism and toxicity assessment in a 3D-liver MPS.

Corresponding Author:

Steven R. Tannenbaum, Department of Biological Engineering, Massachusetts Institute of

Technology, 77 Massachusetts Avenue, Cambridge, MA 02139, Phone: 617- 253-3729,

Fax: 617-252-1787, Email: srt@mit.edu

Statistics:

Number of text pages: 47

Number of tables: 2

Number of figures: 9

Number of references: 49

Number of words in abstract: 244

Number of words in introduction: 750

Number of words in discussion: 1480

Abbreviations:

RMs, reactive metabolites; DCF, diclofenac; LPS, lipopolysaccharide; PK, pharmacokinetics; WEM, William's E media; LC-MS, liquid chromatography-mass spectrometry; PTMs, post-translational modifications; HPLC, high performance liquid chromatography; CAS, chemical abstract service; ACN, acetonitrile; FA, formic acid; DTT, DL-dithiothreitol; IAA, iodoacetamide; QTOF, quadrupole time-of-flight; GCA, glycocholic acid; UHPLC, ultra high performance liquid chromatography; MS/MS, tandem

mass spectrometry; BSA, bovine serum albumin; HSA, human serum albumin; ESI, electrospray ionization; SPI, score peak intensity; IVIVC, in vitro-in vivo correlation; $CL_{int,}$ intrinsic clearance; CL_h, hepatic clearance; f_{ub}, plasma protein binding; APPs, acute phase proteins.

ABSTRACT: *In vitro* hepatocyte culture systems have inherent limitations in capturing known human drug toxicities that arise from complex immune responses. Therefore, we established and characterized a liver immuno-competent co-culture model and evaluated diclofenac (DCF) metabolic profiles, *in vitro-in vivo* clearance correlations, toxicological responses, and acute phase responses using liquid chromatography tandem mass spectrometry. DCF biotransformation was assessed after 48 h of culture, and the major phase I and II metabolites were similar to the *in vivo* DCF metabolism profile in humans. Further characterization of secreted bile acids in the medium revealed that a glycine-conjugated bile acid was a sensitive marker of dose-dependent toxicity in this 3D liver microphysiological system. Protein markers were significantly elevated in the culture medium at high μM doses of DCF, which were also observed previously for acute drug induced toxicity in humans. In this immuno-competent model, lipopolysaccharide treatment evoked an inflammatory response that resulted in a marked increase in the overall number of acute phase proteins (APPs). Kupffer cell-mediated cytokine release recapitulated an *in vivo* pro-inflammatory response exemplified by a cohort of 11 cytokines differentially regulated following LPS-induction, *e.g.,* IL-1β, IL-1Ra, IL-6, IL-8, IP-10, TNF-α, RANTES, G-CSF, M-CSF, MIP-1β, and IL-5. In summary, our findings indicate that 3D liver microphysiological systems may serve as a preclinical investigational platforms from the perspectives of the discovery of a set of clinically relevant biomarkers including potential reactive metabolites, endogenous bile acids, excreted proteins and cytokines to predict early drug-induced liver toxicity in humans.

INTRODUCTION

In the development of drug candidates, experiments with microsomal proteins, S9 fractions, 2D or suspension hepatocytes may not be physiologically sufficient to predict effects in patients. Many patients taking medication may experience chronic or acute inflammation, thus motivating an *in vitro* model that includes liver non-parenchymal cells, especially resident macrophages (Kupffer cells) to capture innate immune responses, including those arising from leaky gut (Roberts et al. 2007). Hepatocytes and Kupffer cells show relatively rapid functional decline in standard culture (Kegel et al. 2015; Godoy et al. 2013), thus a variety of 3D and microperfused cultures that improve *in vitro* physiology have been developed to address complex problems in drug biotransformation, pharmacokinetics (PK), drug-induced liver toxicity, and drug-drug interactions in the early stage of drug development (LeCluyse et al. 2012; Dash et al. 2009; Gómez-Lechón et al. 2004; Li 2007; Kegel et al. 2015; Knospel et al. 2016; Long et al. 2016; Ebrahimhkani et a. 2014). We have developed a microreactor, the LiverChip™, that employs a 0.2 mm thick scaffold to drive formation of 3D tissue-like structures from primary liver cells and an on-board microfluidic pump to provide controlled perfusion to the array of these 3D liver tissue-like structures (Domansky et al. 2010). The recirculation of medium directly through the 3D tissue provides both convective mass transfer of drugs and other molecules to the 3D tissue and results in an approximately physiological drop in oxygen tension from one side of the scaffold to the other. Hepatocytes and Kupffer cells can be co-cultured in a highly functional state in this microreactor for weeks using a culture medium that supports long-term maintenance of cytochrome P450 activity but is also permissive for examining

inflammatory responses (Sarkar et al. 2015; Tsamandouras et al. 2016; Long et al. 2016). The reactor configuration employed here was designed to culture 0.4-0.8 million cells in 1.6-3 mL culture medium, thus providing sufficient sample volume for multiple analyses at multiple time points in order to gain information that could help predict the fate of drugs and their potential toxicity.

Herein, the LiverChip™ culture system was used to study the pharmacokinetics (PK), metabolism, and dose-induced toxicity of diclofenac (DCF), a non-steroidal anti-inflammatory drug and a widely-used painkiller (Tang 2003; Brogden et al. 1980; Skoutakis et al. 1988). As noted by Knöspel et al. in their recent study of DCF metabolism in a larger (1.3 M cells) bioreactor of different configuration (Knöspel et al. 2016), quantitative analysis and comparison of DCF metabolism across different culture formats is challenging, due to effects of mixing [or lack of mixing in static cultures, such as the 3D static spheroids (Messner et al. 2013)] and significant loss of compounds from solution due to adsorption to system components as they observed in their reactor system. Further, DCF binds to plasma proteins, further complicating quantitative interpretation of results. The LiverChip™ system was designed for highly quantitative analysis of exposure and fate, as it is made from components that exhibit minimal adsorption of hydrophobic compounds so that loss of drug is insignificant and exposures can be relatively well-controlled (Tsamandourous et al. 2016; Dash et al. 2009; Long et al. 2016).

DCF metabolism follows two major pathways in humans: (1) phase I: major oxidative metabolite 4'-hydroxydiclofenac and minor 5'-hydroxydiclofenac, and (2) phase II: diclofenac-glucuronide and hydroxydiclofenac-glucuronides, which are toxic due to the formation of reactive electrophilic iso-glucuronides (Bort et al. 1999).

Polarized and well-differentiated hepatocytes synthesize bile acids including amino acid conjugated bile acids (Mörk et al. 2016). Bile acid synthesis may be limited by oxidation, further modification of hepatocytes, or bile transporters (Axelson et al. 2000). They are synthesized from cholesterol by CYP7A1 and, when conjugated, are excreted to the medium (Mörk et al. 2016). Therefore, it is reasonable to speculate that oxidative damage from DCF may alter bile acid metabolism and transport, and thus to investigate bile acid concentrations in conditioned medium as a function of DCF treatment.

Additional insights to the effects of DCF, especially induced by lipopolysaccharides (LPS), can be assessed by both targeted and shotgun proteomics to reveal alterations in known cytokines and acute phase proteins In this study, we investigated secreted protein profiles in cultured medium from cryopreserved hepatocytes and Kupffer cells in a co-culture model.. To investigate whether secreted proteins correlate with toxicity, we exposed the co-culture to a range of doses of DCF with or without a concurrent inflammatory cue (LPS) and profiled large molecules as putative markers of toxicity, including both targeted and shotgun proteomics approaches

MATERIALS AND METHODS

Chemicals and reagents

$^{13}C_6$-DCF and d5-glycocholic acid (GCA), used as internal standards, were obtained from Fluka and Toronto Research Chemicals, respectively. High-performance liquid chromatography (HPLC) grade ($\geq$ 99.9 %) methanol (MeOH, CAS: 67-56-1), acetonitrile (ACN, CAS: 75-05-8), formic acid (FA, CAS: 64-18-6), molecular biology grade dimethyl sulfoxide (DMSO, CAS: 67-68-5), DCF (CAS: 15307-86-5), urea (CAS: 57-13-6),

ammonium bicarbonate (ABC, CAS: 1066-33-7), DL-dithiothreitol (DTT, CAS: 3483-12-3), and iodoacetamide (IAA, CAS: 144-48-9) were purchased from Sigma Aldrich (St. Louis, MO, USA). The standard tuning solution used to calibrate the quadrupole time of flight instrument (QTOF) was acquired from Agilent Technologies (Santa Clara, CA, USA). Distilled water was prepared in-house with double distillation. Trypsin (Catalog# V5111) and protease MAX™ Surfactant (Catalog# V2071) were purchased from Promega (Madison, MI, USA). Albumin depletion kit (Product# 85160) and the top 12 abundant protein depletion spin columns (Product# 85164) were purchased from Life Technologies (Carlsbad, CA, USA). iTRAQ® Reagent - 8Plex Multiplex Kit (SKU#: 4390812) and iTRAQ® Reagent - Multiplex Buffer Kit (SKU# 4381664) were obtained from AB SCIEX (Framingham, MA, USA). OMIX tips (Product # A57003100) and cleanup C18 pipette tips (Product# 5188-5239) were purchased from Agilent Technologies. SPE columns were purchased from Phenomenex (Catalog# 8B-S100-TAK).

Cell Culture

Cryopreserved primary human hepatocytes (Hu8150) and cryopreserved human Kupffer cells (HK8160) were purchased from Life Technologies (Paisley, UK). All cells were thawed according to the manufacturer's instructions. Viability, assessed using trypan blue exclusion post-thaw, was > 85%. Hepatocyte and Kupffer cell co-cultures were seeded into LiverChip™ bioreactors (Long et al. 2016; Kostrzewski et al. 2017) simultaneously at a ratio of 10:1 hepatocytes to Kupffer cells, for a total cell number of 600,000 cells per well, in a volume of 1.6 mL Advanced Dulbecco's Modified Eagle Medium (Ad DMEM) containing thawing and plating supplements (Life Technologies, Paisley, UK), but without

dexamethasone (DEX) for the first 24 h of culture. Flow was maintained in the downward direction at 1.0 µL/sec through the scaffold for 8 h post-seeding and then switched to the upward direction for the duration of culture. From Day 1-3, cultures were maintained in Ad DMEM with primary hepatocyte maintenance supplements, omitting DEX. On Day 3, medium was replaced with William's E Medium (WEM) and maintenance supplements containing 100 nM hydrocortisone (HC). At each medium change, medium samples were saved for analysis of liver-produced proteins (albumin, cytokines) and metabolites (urea). For DCF clearance studies, a complete medium change was performed and DCF (Sigma Aldrich, Poole, U.K.) in DMSO (final concentration of 0.5% v/v for all doses) was added in a volume of 2 mL of medium containing 1.25 mg/mL to yield concentrations indicted in the text. Samples (50 µL each) were removed from duplicate wells at 0, 0.5, 1, 4, 6 24 and 48 h time points. No additional medium was added to replace sample removed. For DCF toxicity, biotransformation, inflammation, and proteomic studies, cultures were dosed with DCF (Sigma Aldrich, Poole, U.K.) in DMSO (final concentration of 0.5% v/v for all doses) on Day 5 to yield initial concentrations indicated in the text, and media were changed every 48 h. At each medium change, fresh compound was added. To induce inflammation, LPS (Sigma, Poole, UK) was dosed at 1 µg/mL.

Characterization of perfused co-cultures in LiverChip™

Quantification of total protein

Cells and scaffolds were washed once in phosphate buffered saline and lysed using 0.5 mL of 0.1 M sodium hydroxide containing 2% sodium dodecyl sulphate. Total cellular

protein was then measured using the Pierce BCA protein assay kit (Thermo Fisher, Loughborough, UK).

Hepatocyte and Kupffer cell phenotyping

Albumin secretion was measured with a human albumin ELISA (Assay Pro, St Charles, USA). Lactate dehydrogenase (LDH) activity was measured using the CytoTox 96® Non-Radioactive Cytotoxicity Assay (Promega, Southampton, UK).

DCF biotransformation

Protein precipitation and extraction of metabolites

Internal standard ($^{13}C_6$-DCF) was added to 25 µL of co-culture medium to give a final concentration of 20 µM of DCF when at 50-100X Cmax (4.4 µM was Cmax for our study), and 2 µM with DCF at 1X Cmax of D5-GCA (0.5 µM to 1 µM) was added as an internal standard prior to sample extraction for bile acid measurements. The choice was arbitrary. 4.4 is a low value in the range of the physiologic dose, and higher values were chosen to represent overdosing. MeOH was then added at a 1:4 ratio (v:v; 25 µL:100 µL; sample:MeOH). Resulting suspensions were maintained at -20 °C for 5 min, vortexed for 20 sec, and subjected to gentle shaking for 5 min on a Fisher Vortex Genie 2 with a vortex adapter. The samples were then maintained at -20 °C for 5 min and centrifuged at 15,000 rpm for 10 min. The supernatants were then collected carefully (without disturbing the protein pellet) and dried in a SpeedVac® (Savant Instruments, Holbrook, NY, USA). Samples were prepared immediately for LC-MS analysis by resuspension in 2% ACN containing 0.1% FA. Injections of 1-5 µL were analyzed on an Agilent QTOF 6530 using

10

parameters described previously (Sarkar et al. 2015).

Metabolite profiling

LC-MS analyses were performed on an Agilent 6530 Accurate-Mass LC-QTOF mass spectrometer with an Agilent Jet Stream Electrospray Ionization (ESI) source and Mass Hunter workstation (v. B.06). The mass spectrometer was interfaced with an Agilent 1290 UHPLC system. The column was an Agilent Extend-C18 (2.1 × 50 mm, 1.8 μm; Agilent Technologies, Santa Clara, CA, USA). The column compartment temperature was set at 40 °C. The QTOF was calibrated daily before runs using the standard tuning solution from Agilent Technologies. ESI mass spectra were acquired in positive ion mode for total and free DCF measurements. Mass data were collected between m/z 70 and 1000 either at 2 scans/sec or 4 scans/sec. The ion spray voltage = 3800 V; the heated capillary temperature = 350 °C; drying gas = 8 L/min; nebulizer = 30 psi; sheath gas temp = 380 °C; sheath gas flow = 12 L/min. Two reference masses (m/z 121.0509: $C_5H_4N_4$; m/z 922.0098: $C_{18}H_{18}O_6N_3P_3F_{24}$) were infused continuously to allow constant mass correction during the run. Variation of retention times and m/z values were ≤ 0.2 min and < 5 ppm mass error, respectively, and the relative standard deviations of peak areas were < 20%. Mobile phases consisted of double distilled water containing 0.1% FA (A) and ACN containing 0.1% FA (B). Linear gradients were from 2% to 95% B over 12 minutes at a flow rate of 0.4 mL/min.

Data processing, analysis, and metabolite identification

DCF clearance and GCA were measured by targeted mass spectrometry on the Agilent QTOF. Data were processed using Agilent Mass Hunter qualitative analysis

software (v. B.06). Peak areas of DCF (*m/z* 296.0245), $^{13}C_6$-DCF, GCA (*m/z* 466.3169), and d5-GCA as internal standard were obtained using the extracted ion chromatogram function. MS/MS spectra of DCF metabolites were analyzed manually with the fragmentor tool in ChemDraw and with the molecular structure correlator function in Mass Hunter (*i.e.,* all signals associated with a given analyte, with intensities > 2000 - 5000, were used to profile metabolites, at a 5 ppm mass accuracy threshold).

Tandem mass spectra (MS/MS) were generated with an Agilent QTOF 6530 mass spectrometer (Santa Clara, CA, USA) to further confirm the identity of metabolites. For this analysis, the matched exact masses of parent and fragmented ions (< 5 ppm mass error), and associated retention times (<20 sec) were used to create a target list. Isotope patterns were also used to identify Cl-containing DCF metabolites.

DCF pharmacokinetics using a one-compartment model

The PK properties of DCF in the LiverChip™ bioreactor were investigated after administration of 4.4 μM DCF to a co-culture of hepatocytes and Kupffer cells (10:1). High mass accuracy LC-MS/MS was used to follow DCF concentrations over time. PK parameters were obtained using MATLAB software (Version R2014, MathWorks Inc., Natick, MA). Based on the initial observation of DCF concentration profile over time, one-compartmental PK model was used to estimate the DCF elimination rate (k_{el}) and the volume of distribution (V_d). Due to sampling from the bioreactor, the V_d was used as the average of the volumes at t=0 and end point. The following equations were used (Eqs. 1 and 2):

$$\frac{dC_{DCF}}{dt} = -k_{el} \times C_{DCF} \qquad \text{(Eq. 1)}$$

$$[C_{DCF}]_0 = \frac{Dose_{DCF}}{V_d} \qquad \text{(Eq. 2)}$$

where C_{DCF} is the DCF concentration, $[C_{DCF}]_0$ is the initial DCF concentration in the liver

bioreactor and $Dose_{DCF}$ is the DCF dose, respectively. The elimination half-life of DCF

($t_{1/2}$) and the clearance (CL) was calculated using equations 3 and 4:

$$t_{1/2} = \frac{\ln(2)}{k_{el}} \qquad \text{(Eq. 3)}$$

$$CL = k_{el}V_d \qquad \text{(Eq. 4)}$$

Modeling of DCF and bovine serum albumin (BSA) equilibrium binding

The binding equilibrium between DCF and BSA (1.25 mg/mL and 25 mg/mL) was

modeled based on the following equation:

$$[DCF_{Bound}] = \frac{n_1 \times k_1 \times [BSA] \times [DCF_{Free}]}{1 + k_1 \times [DCF_{Free}]} + \frac{n_2 \times k_2 \times [BSA] \times [DCF_{Free}]}{1 + k_2 \times [DCF_{Free}]} \qquad \text{(Eq. 5)}$$

where $[BSA]$ is the total BSA concentration, $[DCF_{Bound}]$ and $[DCF_{Free}]$ are bound and free

DCF concentrations, and n_1 and n_2 are the number of binding sites on BSA for DCF, which

are 2.15 and 12.45, respectively (Dutta et al. 2006). Similarly, 0.88×10^5 M^{-1} and $0.727 \times$

10^3 M^{-1} are the association constants k_1 and k_2, respectively. These values were estimated

from the experimental data in Dutta et al.

Protein digestion and peptide fractionation

Prior to digestion, BSA was depleted from the co-culture medium using albumin depletion columns according to the manufacturer's instructions. Proteins were then re-suspended in 15 µL of 8 M urea (dissolved in 50 mM ABC) followed by addition of 20 µL of 0.2% ProteaseMAX^{TM} (Promega) surfactant, 50 µL of ABC (50 mM), and 2.12 µL of 400 mM DTT. Disulfide bonds were reduced by incubating the samples at 56 °C for 30 min, and alkylated by addition of 6 µL of 550 mM IAA, followed by incubation for 30 min at room temperature in the dark. To prevent alkylation of trypsin, excess IAA was inactivated by the addition of 2.12 µL of DTT and incubated for an additional 30 min in the dark. Proteins were digested by adding 3.7 µL of 0.5 µg/µL trypsin (1:27 trypsin:protein) and 1 µL of 1% ProteaseMAX^{TM} followed by a 3 h incubation at 37 °C. After digestion, trypsin was inactivated by addition of 20% trifluoroacetic acid to a final concentration of 0.5%. The tryptic peptides were concentrated and desalted with OMIX tips from Agilent Technologies according to the manufacturer's instructions, and dehydrated to dryness in a SpeedVac$^®$.

To fractionate the peptides by isoelectric focusing, samples were resuspended in 3.6 mL of 1X off-gel buffer and then loaded onto an Agilent off-gel fractionator with IPG strips (pH 3-11) according to the manufacturer's instructions. For the first experiment, the 24 fractions were pooled into 20 fractions (*i.e.,* combining 1 and 24, 2 and 23, 3 and 22, 4 and 21, 5 and 20, without combining fractions 6-19). All fractions were dried in a SpeedVac$^®$ prior to resuspension in 20 µL of 98% water, 2% ACN, and 0.1% FA for LC-MS analysis as described below.

Protein profiling by LC-MS/MS

These experiments were carried out on the Agilent 6530 QTOF mass spectrometer, interfaced with an Agilent 1290 series UHPLC (Agilent Technologies, Santa Clara, CA, USA) containing a binary pump, degasser, well-plate auto-sampler with thermostat, and temperature-controlled column compartment. Mass spectra were acquired in the 3200 Da extended dynamic range mode (2 *GHz*) using the following settings: ESI capillary voltage = 3800 V; fragmentor = 150 V; nebulizer gas = 30 psi; drying gas = 8 L/min; drying temperature = 380 °C. Data were acquired at 6 MS spectra per sec and 3 MS/MS spectra per sec in the mass ranges of *m/z* 100–2000 for MS, and 50-2500 for MS/MS, with a maximum of five precursors per cycle and stored in profile mode. Fragmentation energy was applied at a slope of 3.0 V/100 Da with a 2.8 offset. Mass accuracy was maintained by continually spraying internal reference ions in positive ion mode, *m/z* 121.0509 and 922.0098.

An Agilent ZORBAX 300SB-C18 RRHD column 2.1 × 100 mm, 1.8 μm (Agilent Technologies, Santa Clara, CA, USA) was used for all analyses. The LC parameters were the following: autosampler temperature = 4 °C; injection volume = 20 μL; column temperature = 40 °C; mobile phases were 0.1% FA in water (A) and 0.1% FA in ACN (B). The gradient started at 2% B at 400 μL/min for 1 min, increased to 50% B from 1 to 19 min with a flow rate of 250 μL/min, then increased to 95% B from 19 to 23 min with an increased flow rate of 400 μL/min and held up to 27 min at 95% B before decreasing to 2% B at 27.2 min, ending at 30 min and followed by a 2 min post run at 2% B.

Proteomics data processing

Raw data were extracted and searched with the Spectrum Mill search engine (B.04.00.127, Agilent Technologies, Palo Alto, CA, USA) using published parameters

15

(Ravindra et al. 2015). Protein expression values (spectrum counts) were determined with Scaffold software using the imported peptide hits from Spectrum Mill. The threshold for considering a protein identification included a minimum of two distinct peptides with 95% confidence.

iTRAQ 8plex: protein digestion, labeling, and chromatography

The albumin was depleted prior to processing the samples for iTRAQ labeling. For these experiments, 100 µg total protein from individual samples was reduced in 2 mM of tris(2-carboxyethyl)phosphine at 37 °C for 30 min, and the cysteine residues were blocked in 10 mM methyl methanethiosulfonate at room temperature for 1 h, followed by trypsin digestion (modified trypsin from Promega) at a protease: protein ratio of 1:40 (w:w) at 37 °C overnight. iTRAQ-8plex labeling reagents were added to the peptide samples, which were incubated at room temperature for 3 h with the addition of isopropyl alcohol. The reaction was stopped by the addition of 10 mM monopotassium phosphate, 25% ACN, pH 2.6 (solvent A), followed by centrifugation at 14000 × g for 10 min to remove aggregated proteins. All individual samples were pooled and purified using SPE columns prior to fractionation. Then, digested protein samples were separated by using the Agilent 3100 OFFGEL fractionator along 3-11 pH range into 24 fractions based on peptide isoelectric points. The individual fractions were collected and concentrated in a SpeedVac® before MS analysis. Individual fractions were further cleaned with C18 pipette tips. All identified proteins, as well as their spectral counts and quantitative values, are shown in Table 1 and Supplemental Table 1.

Cytokine analysis

Multiplex immunoassays

Determination of 62 unique cytokines, chemokines, growth factors, and matrix metalloproteinases was performed using the human group 1 27-plex and 40-plex chemokine panels, as well as select singleplexes of group II 21-plex and inflammation panel 1 37-plex (Supplemental Fig. 1). Assays were completed according to the manufacturer's instructions (BioRad Laboratories, Hercules, CA, USA), with the exception that coupled beads, biotinylated detection antibodies, and streptavidin-phycoerythrin fluorescent reporters were diluted 2-fold. All analytes were evaluated in neat, undiluted samples; a total volume of 50 µL sample from co-culture medium was analyzed per multiplex panel. To attain a measurement for IL-8 within the working range of the assay, samples were diluted 8-fold. Standard and sample diluents consisted of WEM (Life Technologies, Carlsbad, CA, USA) in the presence of 0.75% BSA (Sigma-Aldrich, St. Louis, MO, USA) as a final concentration.

Assays were performed in parallel (unmixed) to avoid antibody cross-reactivity between groups. Prepared arrays were assessed by the 3D suspension array system (BioRad Laboratories, Hercules, CA, USA) utilizing xMAP technology licensed by Luminex. Data were collected with xPONENT for FLEXMAP 3D software, version 4.2 (Luminex Corporation, Austin, TX, USA) and results were evaluated initially in BioPlex Manager Software version 6.1 (BioRad Laboratories, Hercules, CA, USA). Median fluorescence intensity values were converted to absolute concentrations via calibration to fifteen-point standard series that implemented a 2-fold serial dilution. Assay performance metrics for each analyte are summarized in Supplemental Table 2.

Data processing and statistical analyses

To quantify the concentration of each analyte, the five-parameter (5PL) logistic model was used for the best curve fit of standards. Regression analysis minimized the weighted sum of squared errors (wSSE). In general, the weights are set equal to the inverse variance; however, for immunoassays, the high-response end of a curve approaches saturation of the detector thus variance is approximated more appropriately by a power function,

$$\text{variance} = A(\text{response})^B \qquad\qquad \text{(Eq. 6)}$$

where A is a function of the magnitudes of the responses and $1.0 \leq B \leq 2.0$ for immunoassays (Finney 1987). Curve-fitting techniques were completed in BioPlex Manager Software version 6.1 (BioRad Laboratories, Hercules, CA, USA). Parameters including wSSE, residual variance, and fit probability are provided (Supplemental Table 2).

Multivariate statistical techniques, such as unsupervised hierarchical clustering, were evaluated in MATLAB version 2012b (Mathworks Inc, Natick, MA, USA).

Bioinformatics

GO and KEGG pathway enrichment analyses ($P > 0.05$) were performed by using the functional annotation tool DAVID (Huang et al. 2009). A professional software ClueGO, Cytoscape plug-in (Bindea et al. 2009), was used to facilitate identification of the functional and pathway analyses for DCF and LPS treated hepatocyte culture medium.

RESULTS

Concentration-depending binding equilibrium of DCF and BSA

DCF in plasma exists in equilibrium between free and albumin-bound forms, with the free form available for metabolism (Dutta et al. 2006; Zhang et al. 2015). Albumin contains multiple different binding sites for lipophilic compounds hence equilibrium binding can be a complex function of concentration with multiple molecules of drug bound to the same albumin molecule in sites of different affinities, competing with other lipophilic molecules like steroid hormones (Dutta et al. 2006). DCF equilibrium with albumin has been fit to a model comprising 2 high affinity and 12 low-affinity sites (Dutta et al. 2006; see Methods). Chemically-defined liver cell culture media often contain BSA or other albumin sources as carriers of lipophilic nutrients. Although the normal human plasma concentration of albumin is 35-55 gm/L (530 μM), lower albumin concentrations, in the range of 1 -10 gm/L (15-150 μM) are typically used in cell culture. Even at these lower concentrations, the presence of albumin can influence the free concentration of drugs present, affecting the PK properties. We thus assessed these equilibria experimentally across our dose range in order to build appropriate PK models of our experimental clearance and metabolism data using our culture media, which contains other albumin-binding lipophilic molecules including cortisol. We first built a binding landscape from published data (Zhang et al. 2015) (Fig. 1A), illustrating the non-linear nature of binding to two sites on albumin. We then experimentally determined the DCF-albumin binding equilibria in the culture medium used for the clearance and metabolism studies in this work and found that measured outcomes were in agreement with the literature for the 1.25 gm/L BSA concentration used

in these studies and total DCF concentrations up to 100 µM (Fig. 1B). Hence, the binding

curve described in Methods was used for further PK analysis.

Baseline DCF clearance and metabolism in the LiverChip™

Duplicate wells of co-cultured hepatocytes and Kupffer cells in standard media

containing 1.25 gm/L BSA were examined for two doses of DCF. Medium samples were

collected and analyzed as described in Methods. We first confirmed that DCF exhibited no

detectable binding to the LiverChip™ components by dosing LiverChip™ wells in the

absence of cells and monitoring the concentration over 24 h (data not shown). This finding

is in concordance with previous reports that the LiverChip™ exhibits low drug-binding

(Tsamandouras et al. 2016).

Drug clearance was quantified after dosing with a pharmacological 4.4 µM dose and

a suprapharmacological 440 µM dose of DCF in medium containing 1.25 gm/L BSA (Fig. 2

A-B, and Supplemental Table 3. Clearance parameters were calculated from the

concentration profiles of total DCF as a function of time, taking into account the reactor

mixing properties and albumin binding, using a PK model as described in Methods. The $t_{1/2}$

of DCF at a pharmacological dose of was estimated to be 14.6 h in the LiverChip™

bioreactor. Clearance was also investigated at a higher dose, 440 µM (Fig. 2B) as this

condition was used to assess metabolite production in addition to clearance.

Extrapolation of *in vitro* DCF clearance data to predict intrinsic clearance

In vivo-in vitro correlation (IVIVC) provides valuable information for the first in

human dosing. Here, the retrospective IVIVC analysis of the DCF clearance using $t_{1/2}$ and

V_d to calculate intrinsic clearance (CL_{int}) by accounting for the scaling factors detailed in

Eq. 7 (Davies and Morris 1993; Obach et al. 1997; Obach et al. 1999; Sarkar et al. 2015):

$$CL_{int} = \frac{ln2}{t_{1/2}} \times \frac{liver\ weight}{standard\ body\ weight} \times \frac{V_d}{hepatocytes/well} \times hepatocytes\ /g\ liver \quad \text{(Eq.7)}$$

Values of scaling parameters and intrinsic clearance are found in Supplemental

Table 3. The predicted CL_h was 0.55 mL/min/kg, which is < 7-fold underpredicted than *in

vivo* plasma clearance (3.8 mL/min/kg) (data also available at www.capkr.man.ac.uk).

Although predicted CL_h is generally underpredicted for DCF, and the contribution of gut

and other organs need to be considered to get better predicted plasma clearance in human

(Hallifax et al. 2010; Brown et al. 2007).

Assessment of toxicity of DCF in the LiverChip™

The toxicity of DCF in the LiverChip™ was assessed using a 5-point dose response

with three times 48 h doses given starting at Day 5 (i.e., dosed on Day 5, 7, and 9). Cell

viability was assessed using WST-1 reagent 48 h after the third dose (Fig. 3A) resulting in

an IC50 for the primary hepatocyte-Kupffer cell co-cultures in LiverChip™of 227 µM. This

is comparable to the IC50 for DCF generated from spheroid culture of primary hepatocytes

and non-parenchymal cells (Messner et al. 2013). To evaluate the temporal reduction in

function and cell death over the multiple DCF doses, LDH (Fig. 3B) and albumin (Fig. 3C)

were measured 48 h after each dose. Throughout the culture period, vehicles controls (0.1%

v/v DMSO) showed sustained levels of albumin secretion indicating that hepatocytes in the

co-cultures remained functional. At high DCF concentrations (> 50X) albumin secretion declined after a single dose, while LDH release became more pronounced after the second dose. Co-dosing of LPS resulted in the production of pro-inflammatory cytokines TNFα and IL-6 (data not shown) but that result does not significantly change the toxicity profile of DCF as assessed by gross markers of functionality and cell death.

DCF biotransformation by phase I and II metabolism under basal and inflamed conditions

Accurate masses, MS/MS, and available standards corresponding to major DCF metabolites from liver co-culture system were used to elucidate structures. Extracted ion chromatograms (EIC)% values of metabolites were only used to understand the relative amounts formed in this co-culture system.

We observed 4-hydroxy-DCF and 5-hydroxy DCF as major, and minor phase I metabolites, respectively; and acylglucuronides of DCF, hydroxy-DCF, and DCF-sulfate as major phase II metabolites (Fig. 4). UGT and SULT activities were confirmed to be stable in this human liver model as measured by DCF phase II metabolites. Under the culture conditions, three glucuronides of DCF and hydroxylated DCF were observed which might be a result of isomeric acylglucuronides.

As assessed by the production of 4-hydroxy-DCF, CYP2C9 activity on Day 5 was found to be 1.5-fold greater than Day 7. A minor methoxylated hydroxy DCF metabolite was detected and found to be approximately 2.8-fold higher when the LiverChip™ when treated with drug and LPS in combination. Using our LC-MS method, we did not observe

GSH-DCF related adducts in the culture medium. Minor metabolites were putatively predicted by ≤ 5 ppm mass accuracy and chlorine isotopic signature.

Co-treatment with LPS down-regulated 2-fold the CYP450-dependent formation of 4-hydroxy-DCF, 1.5-fold up-regulated UGT-dependent formation of total DCF-acylglucuronides, 2.4-fold of total hydroxylated-DCF acyl glucuronides, and no significant changes in sulphonated product was observed (data not shown). The assignment of human P450 enzymes to the formation of phase I and II DCF metabolites in this liver MPS is based on previous work by Boelsterli et al. 2003 and Tand et al. 2003.

Endogenous glycocholic acid (GCA) as a model bile acid marker of DCF induced toxicity

The liquid chromatography/mass spectrometry methods developed for the analyses of HC and DCF capture data for all compounds in the solutions that are present in detectable amounts. Analysis of this data with software allows untargeted searches and extracts molecular weights for detectable compounds in the media, and highlights those, which change with various experimental conditions. The molecular weights for compounds in these subsets can then be searched against databases that suggest possible structures, and some of these can be identified by interpreting the mass spectra from these compounds. In this instance, a prominent compound that decreased with drug treatment was identified as the bile acid GCA. This in turn suggested a targeted search - of the same data sets - for other bile acids, several of which were detected and putatively identified based on mass accuracy (< 5-10 ppm), and some available standards (Fig. 5). These also declined in concentrations following treatment with DCF at various levels, and due to the unavailable reference

standards, the formation of other detected bile acids were determined by accurate mass spectrometry area units. GCA was considered as a model bile acid in this 3D liver culture. Peak intensity (EIC%) relative values were for guidance only. They do not represent absolute amounts present in these experiments. GCA peak area was considered as 100 and the relative EIC without DCF, and DCF were listed for other detected bile acids (Table 2). The extracellular concentration of GCA in the absence of DCF was found to be 3- 4 µM, and there is a constant level in the system for up to two weeks. No GCA was detected in the starting medium at zero time point, indicating that GCA was synthesized by the 3D LiverChip™ system. The Cmax for the recommended dose of DCF in humans is 4.4 µM and experiments were carried out up to 100 Cmax. Over a wide range of concentration, there is a continuous dose-response relationship for DCF induced toxicity as assessed by suppression of GCA production (Fig. 6A). Figure 6B demonstrates the effect of LPS alone and together with DCF, showing that there is a synergistic effect of inflammation on drug toxicity. This effect provides subtle early indications of impaired liver function that precedes cell death.

Secreted proteins as toxicity markers

In most of our study we focused on high dose (440 µM) DCF-treated culture medium. Prior to processing the samples, albumin was depleted from culture medium, then analyzed by shotgun proteomics and quantified by spectral counting. Here, we refer to albumin as BSA provided within commercial medium. All detectable proteins from culture medium were searched against the NCBInr human proteome database using Agilent Spectrum Mill. Proteins identified are listed in Supplemental Table 1.

Spectral counting of experimental data indicated a significant difference between samples treated with 440 μM DCF and assessed on Day 5 compared to Day 7 (Fig. 7A and B). Fifty-four proteins were common between the control and the DCF culture medium on Day 5, while only 13 proteins were different between the control and DCF treated samples (Fig. 7A). In contrast, the Venn diagram in Fig. 7B illustrates that 52 proteins are common between the control and DCF treated samples on Day 7. Notably, the high dose of DCF treatment elevated an additional 68 proteins, which are not identified in the control. However, between Day 5 and 7 of dosed culture medium, nearly 53 proteins were common and nearly 67 proteins were highly elevated in Day 7 (Fig. 7C).

The pie chart in Fig. 7D shows that nearly 66% of the proteins were released into the medium, most of which are regulated by the intrinsic apoptotic-signaling pathway in response to oxidative stress. Another 24% are from the cellular aldehyde metabolic process. Of the 120 hepatic proteins identified in culture medium, 45% were intracellular or membrane proteins, 21% were plasma proteins, 12% were ECM proteins, and 22% were identified as miscellaneous (Fig. 7E).

Functional analysis by assessing secreted proteins under inflammatory conditions

Secreted proteins under LPS-induced inflammation were identified and quantified using iTRAQ-based LC-MS/MS (Supplemental Table 4). The selected positive and negative APPs are listed in Table 1. Figure 8 A-C shows the Venn diagrams of the major APPs (19 selected proteins) compared among three different conditions at Day 7. Sixteen APPs are common between control and LPS, with only 3 additional proteins evoked during LPS treatment (Fig. 8A). Between control and the drug treatment only 7 APPs are common

25

between the two sets (Fig. 8B), but the high concentration of drug completely suppressed the secretion of APPs. In comparison between LPS and LPS with DCF, only 8 APPs are common to the two treatments, another 12 are present in only LPS-treated conditioned medium.

The selected APPs quantitative values are listed in Table 1. The drug and LPS treatment samples were normalized to control samples. The LPS with drug treatment samples were normalized to only LPS treated conditioned medium. The treatment of LPS increases the production of all the APPs, but most of the APPs secretion were decreased by the addition of drug. Of the identified proteins in LPS-treated conditioned medium approximately 50% are secreted into the medium due to the acute phase response following LPS treatment. Another 23% were associated with high-density lipoprotein particle clearance. The GO cellular component analysis indicates that these proteins are derived from the extracellular matrix and region, membrane, and organelle compartment of the cells.

LPS-mediated cytokines profiles in hepatocyte:Kupffer cell co-cultures

By incorporating components of the innate immune system, *i.e.,* Kupffer cells, we determined cytokine profiles of LPS-induced inflammation using an *in vitro* model that is more physiologically relevant than hepatocyte monocultures. To investigate the coherent "signature" of inflammation due to this specific stimulus, multiplexed bead-based immunoassays enabled the assessment of 62 unique cytokines, chemokines, growth factors, and metalloproteinases; 31 secreted factors were greater than the limit of detection (Supplemental Table 2). In the absence of LPS stimulation, fewer cytokines, chemokines, and growth factors were detectable in the culture medium and therefore eliminated for

further analyses (Supplemental Table 2). For proteins detectable in all conditions, concentrations (pg/mL) were normalized by total protein to account for well-to-well variability on the LiverChip™; experiments (± 1 µg/mL LPS) were carried out in duplicate.

Multivariate analysis identified a cohort of 11 pro-inflammatory cytokines (TNF-α, RANTES, G-CSF, IL-8, IL-6, M-CSF, IL-1β, MIP-1β, IP-10, IL-5, and IL-1Ra) that correlate to LPS-induced inflammation. Unsupervised hierarchical clustering distinguishes these secreted factors while emphasizing reproducibility between experimental replicates (Fig. 9A). Consistent with recent findings, the treatment of co-cultures (10:1, hepatocytes:Kupffer) with LPS for 24 h resulted in substantially higher release of proinflammatory cytokines (TNF-α, IL-8, IL-6, and IL-1β) into culture medium compared with untreated co-cultures (Fig. 9B) (Nguyen et al. 2015). We further identified significant increases in secretion of RANTES, G-CSF, and Eotaxin-3, and to a lesser degree, MIP-1α, M-CSF, MIP-1β, IL-5, and IP-10 (Fig. 9B and C). This in-depth characterization of molecular signatures differentiated a distinct cytokine profile associated with decreased levels of select analytes that was reproducible among experimental replicates (Fig. 9D). Figure 9E shows the fold-change values for each analyte based on the LPS-stimulated or un-stimulated results.

DISCUSSION

As previously observed for this bioreactor (Long et al. 2016; Wheeler et al. 2014), albumin, CYP3A, total protein, glucose, and urea production were stable in LiverChip™ cultures, indicating viability, survival, and preservation of the hepatic CYP3A4 isoforms were previously shown to be active on Days 7-10 in co-cultures (Sarkar et al. 2015). Since

drug-plasma protein binding is a major factor influencing bioavailability of this drug the binding kinetics between DCF and albumin from media were measured, revealing significant effects on DCF half-life in the range of 1.25 mg/mL to 25 mg/mL BSA.

We also confirmed that there was insignificant loss of DCF due to adsorption to the bioreactor components, in contrast to what was observed in a recent bioreactor study of DCF fate (Knospel et al. 2016). This enabled quantitative analysis of DCF fate when measurements are combined with detailed models of plasma protein binding. As we and others have reviewed comprehensively elsewhere (Ebrahamkhani et al. 2014; LeClusyse et al. 2012; Gody et al. 2013), the added complexity and expense of bioreactor culture make it desirable for relatively challenging problems where long-term function and co-cultures are required to illuminate responses. An earlier study of hepatocyte – Kupffer cell interactions in DCF toxicity, using standard 2D culture, illustrated the rapid decline in function of primary cells, and limited the ability to carry out co-exposures and to examine the comprehensive range of responses we were able to study here (Messmer et al. 2013).

DCF metabolites including 4-hydroxy and 5-hydroxy DCF as major and minor phase I metabolites, respectively; and acylglucuronides of DCF, hydroxy-DCF, and DCF-sulfate as major phase II metabolites, were observed (Fig. 4). These metabolites were accounted for by CYP2C9, CYP2C8, and UGT2B7 metabolism, although under our assay conditions four glucuronide isomers of DCF and hydroxy-DCF were observed which may suggest the potential involvement of other isoform phase II enzymes.The formation of 4-hydroxy-DCF is mediated by CYP2C9; both DCF and its oxidative metabolites undergo glucuronidation and sulfation (Boelsterli et al., 2003 and Tand et al., 2003).

LPS can alter gene expression, while combinations of LPS with DCF may further

regulate concentrations of proinflammatory cytokines and markers of cell death Under our conditions, DCF plus LPS exhibited a lower half-life, supporting the hypothesis that stress can induce oxidative stress-mediated pathways, which are independent of the formation of electrophilic metabolites, and play a role in drug metabolism.

While polarized and well-differentiated hepatocytes can synthesize physiologically relevant conjugated bile acids; their synthesis could be limited by oxidation and stress. Bile acids are synthesized primarily from cholesterol by CYP7A1, and all bile acids are conjugated and actively excreted (Schwartz et al. 2001). These conjugated bile acids can be up taken by hepatocytes as part of bile acid transport in a physiologically-relevant *in vitro* model (Mörk et al. 2016). We characterized the level of bile acids as a function of DCF treatment-and a glycine-conjugated bile acid, GCA, was found to be a marker for DCF dose-dependent early toxicity. The decrease of bile acid synthesis correlated with the suppression of cholesterol 7 alpha-hydroxylase (CYP7A1).

To achieve a greater depth in characterizing these models we took a quantitative mass spectrometry approach and used several methods to reduce the inherent complexity of the conditioned medium before processing the samples for proteomic analysis. Two high-abundant proteins (albumin and IgG) were removed prior to sample processing. Within the networks of closely associated proteins, differentially expressed genes were explored using cytoscape analysis, ClueGO; especially those associated with toxicity and acute phase response. The number of proteins identified at 100 Cmax (Cmax = 4.4 µM for this study) in the early stage of drug treatment is relatively small (Fig. 7A). At Day 7, however, increased numbers of proteins were identified in the DCF treated samples (Fig. 7B and C; Supplemental Table 1).

This indicates a delay of the toxic response from Day 5 to Day 7 as measured by protein leakage. A toxic concentration of DCF caused significant cell death accompanied by leakage of numerous cytoplasmic proteins. Gene Ontology annotation revealed that these proteins were distributed across different cellular components and were secreted due to oxidative stress (Fig. 7D and E) and that few of them are involved in the metabolic process. Known markers of hepatotoxicity, e.g., alcohol dehydrogenase 4 [ADH4], aspartate aminotransferase [AST], aldo-keto reductases, and Cu/Zn-superoxide dismutase were detected at Day 7 with higher doses of DCF. Some metabolic enzymes such as carbonic anhydrase, glucose-6-phosphate isomerase, glutathione-s-transferase, and protein disulfide isomerase were also identified on Day 7. Our data also suggest that the hepatocytes are actively remodeling their environment, since we identified several structural extracellular matrix proteins as well as some proteins known to be secreted during liver regeneration.

LPS was added to the circulating media in order to elicit an inflammatory response resulting in increased protein levels of many acute-phase proteins. These proteins were initially confirmed by shotgun proteomics and then quantitated using iTRAQ labeling. Identified proteins belong to the medium-to-high abundance APPs and were used to compare protein synthesis in different experiments. iTRAQ analysis of co-culture conditioned medium revealed the major reduction in overall APPs synthesis by the addition of DCF (Fig. 8B, 8C, and Table 1) with the exception of amyloid beta A4 protein isoform b. Interestingly, there is significant difference between the LPS and drug treatment on the expression of the APPs (Table 1). We expected that the DCF exposure to the hepatocytes would increase the expression of APPs; but that was not the case. For example, exposure of carbon tetrachloride to rats decreases the expression of α2-macroglobulin (Fountoulakis et

al. 2002) suggesting that a decrease in APP could be a marker of toxicity. It is possible that DCF causes toxicity through the down-regulation of these proteins by leading to uncontrolled breakdown of liver tissue. That may be reason the genetic deficiency in α1-antitrypsin is one of the risk factor in development of hepatocellular carcinoma (Blum 2002). Drug-treated cells did not resume production of these proteins even after exposure to LPS, supporting the results from other studies using proteomic based measurements, where drug treatment affects the APPs synthesis in hepatocytes cultured in collagen sandwiches. Nearly 50% of proteins released into the medium at Day 7 are involved in the LPS-related acute phase response. The other half are involved in the high density lipoprotein particle clearance, negative regulation of endopeptidase and oxidoreductase activity, kariocyte differentiation, retinol homeostasis, and protein stabilization. Subcellular localization analyses revealed that most proteins are localized in the membrane and nucleus.

Pro-inflammatory cytokines such as TNF-α, interleukin 1 beta (1L-1β), and IL-6 can induce acute and chronic liver damage. Following high drug dose or long term repeated therapeutic dose, TNF-α, 1L-1β, and IL-6 are released into the bloodstream from liver during drug induced hepatic injury. We evaluated differential regulation of cytokine secretion in the culture media due to high dose of drug-induced injury and whether these profiles were potential biomarkers of *in vivo* human liver drug induced toxicity.

In the presence of Kupffer cells, we detected 31 of 62 cytokines whose profiles were assessed in the absence or presence of LPS at 24 h. Eleven pro-inflammatory cytokines [TNF-α, RANTES, G-CSF, IL-8, IL-6, M-CSF, IL-1β, MIP-1β, IP-10, IL-5, and IL-1Ra] correlate to LPS-induced inflammation. We also identified increases in the secretion of

RANTES, G-CSF, and Eotaxin-3, and to a lesser degree: MIP-1α, M-CSF, MIP-1β, IL-5, and IP-10.

The pro-inflammatory effect of IL-1β is likely due to its synergism with toll-like receptor (TLR) signaling, which markedly amplifies inflammation via LPS-inducible cytokines (Szabo et al. 2015). LPS signals through TLR4, and appears to be the initial signal that induces IL-1β expression (Petrasek et al. 2012; Miura et al. 2010). The secretion of IL-1β is specific to Kupffer cells (Petrasek et al. 2012), and mediates cytokines and chemokines including TNF-α and MCP-1 (Mandrekar et al. 2011; Granowitz et al. 1992; Dinarello 2009), respectively, and recruits inflammatory cells to the liver during disease progression (Mehal 2010). In addition to IL-1β, elevated signals produced by Kupffer cells were observed for MIP-1β and IL-8. Taken together, cytokine release data confirmed that Kupffer cells are present and functional at Day 7, *i.e.,* 24 h following LPS induction.

Collectively, functional analyses in a non-invasive way such as LDH release, total protein per well, albumin secretion, phase I and II biotransformation, cytokine profiling and proteomics based toxicity results demonstrated that this system is capable of recapitulating DCF metabolism, and escalated dose induced toxicity in the human liver. This platform can be a valuable tool in the different phases of the drug development processes (fit for purpose utility) to predict *in vivo* drug biotransformation, PK, and drug-induced hepatotoxicity (*i.e.,* adverse effects). Each small molecule, however, may behave differently *in vivo* from the perspectives of pharmacokinetics, pharmacodynamics, and types of diseases. Additional experimental optimizations, based on low to moderate to high clearance compounds, are consequently needed to develop a more accurate and predictive human-cell-based *in vitro* MPS.

ACKNOWLEDGEMENTS

AUTHORSHIP CONTRIBUTIONS

Participated in research design: US, KCR, CY, EL, JY, MC, DJH, LGG, DAL, JSW, SRT

Conducted experiments: US, KCR, EL, CY

Performed data analysis: US, KCR, CY, DJH, JY, MC, DRB, JSW

Wrote or contributed to the writing of the manuscript: US, KCR, DRB, DJH, CY, JY, MC, JSW, LGG, SRT

<u>REFERENCES</u>

Axelson M, Ellis E, Mörk B, et al (2000) Bile acid synthesis in cultured human hepatocytes: support for an alternative biosynthetic pathway to cholic acid. Hepatology 31:1305–1312. doi:10.1053/jhep.2000.7877

Bindea G, Mlecnik B, Hackl H, et al (2009) ClueGO: a Cytoscape plug-in to decipher functionally grouped gene ontology and pathway annotation networks. Bioinformatics 25:1091–1093. doi: 10.1093/bioinformatics/btp101

Blum, HE (2002) Molecular targets for prevention of hepato- cellular carcinoma. Dig. Dis. 20,81-90.

Boelsterli et al., 2003. Diclofenac-induced liver injury: a paradigm of idiosyncratic drug toxicity. Toxicol and Appl Pharmacol. ;192(3):307-322

Bort R, MacÉ K, Boobis A, et al (1999) Hepatic metabolism of diclofenac: Role of human CYP in the minor oxidative pathways. Biochem Pharmacol 58:787–796.

Brogden RN, Heel RC, Pakes GE, et al (1980) Diclofenac sodium: a review of its pharmacological properties and therapeutic use in rheumatic diseases and pain of varying origin. Drugs 20:24–48.

Brown HS, Michael Griffin M, Houston JB (2007) Evaluation of Cryopreserved Human Hepatocytes as an Alternative in Vitro System to Microsomes for the Prediction of Metabolic Clearance. Drug Metabolism and Disposition 35:293-301

Dash A, Inman W, Hoffmaster K, Sevidal S, Kelly J, Obach RS, Griffith LG, Tannenbaum SR (2009) Liver tissue engineering in the evaluation of drug safety. Expert Opin Drug Metab Toxicol. 2009 Oct;5(10):1159-74.

Davies B, Morris T (1993) Physiological parameters in laboratory animals and humans. Pharm Res 10:1093–1095.

Dinarello C (2009) Immunological and inflammatory functions of the interlukin-1 family. Annu Rev Immunol 27:519-550.

Domansky K, Inman W, Serdy J, Dash A, Lim MH, Griffith LG (2010) Perfused multiwell plate for 3D liver tissue engineering. Lab Chip 10(1):51-8. doi: 10.1039/b913221j. Epub 2009 Oct 22.

Dutta SK, Basu SK, Sen KK (2006) Binding of diclofenac sodium with bovine serum albumin at different temperatures, pH and ionic strengths. Indian J Exp Biol 44(2):123-7.

Ebrahimkani M, Shepard J, Raredon MS, Hughes D, Griffith L.G (2014) Bioreactors to Support Liver Function in Vitro. Advanced Drug Delivery Reviews, 69-70:132-57.

Finney D.J (1987) Statistical Method in Biological Assay (3rd ed.). London: Griffin.

Fountoulakis M, de Vera MC, Crameri F, Boess F, Gasser R, Albertini S, Suter L (2002) Modulation of gene and protein expression by carbon tetrachloride in the rat liver. Toxicol. Appl. Pharmacol. 183,71-80.

Godoy P, Hewitt NJ, Albrecht U, Andersen ME, Ansari N, Bhattacharya, S et al. (2013) Recent advances in 2D and 3D in vitro systems using primary hepatocytes, alternative hepatocyte sources and non-parenchymal liver cells and their use in investigating mechanisms of hepatotoxicity, cell signaling and ADME. Arch. Toxicol. 87, 1315–1530.

Gómez-Lechón MJ, Donato MT, Castell J V, Jover R (2004) Human hepatocytes in primary culture: the choice to investigate drug metabolism in man. Curr Drug Metab 5:443–462.

Granowitz EV, Clark BD, Vannier E, Callahan MV, Dinarello CA (1992) Effect of interleukin-1 (IL-1) blockade on cytokine synthesis: I. IL-1 receptor antagonist inhibits IL-1-induced cytokine synthesis and blocks the binding of IL-1 to its type II receptor on human monocytes. Blood 79(9):2356-63.

Hallifax D1, Foster JA, Houston JB (2010) Prediction of human metabolic clearance from in vitro systems: retrospective analysis and prospective view. Pharm Res (10):2150-61.

Huang DW, Sherman BT, Lempicki R a (2009) Systematic and integrative analysis of large gene lists using DAVID bioinformatics resources. Nat Protoc 4:44–57.

Kegel V, Pfeiffer E, Burkhardt B, Liu JL, Zeilinger K, Nüssler AK, Seehofer D, Damm G (2015) Subtoxic Concentrations of Hepatotoxic Drugs Lead to Kupffer Cell Activation in a Human In Vitro Liver Model: An Approach to Study DILI. Mediators Inflamm 2015:640631. doi: 10.1155/2015/640631. Epub 2015 Sep 28.

Knöspel F, Jacobs F, Freyer N, Damm G, De Bondt A, van den Wyngaert I, Snoeys J, Monshouwer M, Richter M, Strahl N, Seehofer D, Zeilinger K (2016) In vitro model for hepatotoxicity studies based on primary human hepatocyte cultivation in a perfused 3D bioreactor system. Int J Mol Sci 2016 Apr 16;17(4):584.

Kostrzewski T, Cornforth T, Snow SA, Ouro-Gnao L, Rowe C, Large EM, Hughes DJ (2017) Three-dimensional perfused human in vitro model of non-alcoholic fatty liver disease. World J Gastroenterol. 2017 Jan 14; 23(2): 204–215.

LeCluyse EL, Witek RP, Andersen ME, Powers MJ (2012) Organotypic liver culture models: meeting current challenges in toxicity testing. Crit. Rev. Toxicol. 42, 501–548.

Li AP (2007) Human hepatocytes: Isolation, cryopreservation and applications in drug development. Chem Biol Interact 168:16–29.

Long TJ, Cosgrove PA, Dunn II RT, Stolz DB, Hamadeh H, Afshari C, McBride H, Griffith LG (2016) Modeling therapeutic antibody-small molecule drug-drug interactions using a three-dimensional perfusable human liver coculture platform. Drug Metab Dispo 44: 1940-1948.

Mandrekar P, Ambade A, Lim A, Szabo G, Catalano D (2011) An essential role for monocyte chemoattractant protein-1 in alcoholic liver injury: regulation of proinflammatory cytokines and hepatic steatosis in mice. Hepatology 54(6):2185-97.

Mehal W, Imaeda A. (2010) Cell death and fibrogenesis. Semin Liver Dis. 30(3):226-31.

Messner S, Agarkova I, Moritz W, Kelm JM (2013) Multicell type human liver microtissues for hepatotoxicity testing. Arch Toxicol. 2013 Jan;87(1):209-13. doi: 10.1007/s00204-012-0968-2. Epub 2012 Nov 11.

Miura K, Kodama Y, Inokuchi S, Schnabl B, Aoyama T, Ohnishi H, Olefsky JM, Brenner DA, Seki E (2010) Toll-like receptor 9 promotes steatohepatitis by induction of interleukin-1beta in mice. Gastroenterology 139(1):323-34.

Mörk LM, Strom SC, Mode A, Ellis EC (2016). Addition of dexamethasone alters the bile acid composition by inducing CYP8B1 in primary cultures of human hepatocytes. J Clin Exp Hepatol. 6(2):87-93.

Nguyen TV, Ukairo O, Khetani SR, McVay M, Kanchagar C, Seghezzi W, Ayanoglu G, Irrechukwu O, Evers R. (2015) Establishment of a hepatocyte-kupffer cell co-culture model for assessment of proinflammatory cytokine effects on metabolizing enzymes and drug transporters 43(5):774-85.

Obach RS, Baxter JG, Liston TE, et al (1997) The prediction of human pharmacokinetic parameters from preclinical and in vitro metabolism data. J Pharmacol Exp Ther 283:46–58.

Obach RS (1999) Prediction of human clearance of twenty-nine drugs from hepatic microsomal intrinsic clearance data: an examination of in vitro half-life approach and nonspecific binding to microsomes. Drug Metab Dispos **27**:1350–1359

Petrasek J, Bala S, Csak T, et al (2012) IL-1 receptor antagonist ameliorates inflammasome-dependent alcoholic steatohepatitis in mice. J Clin Invest 122(10):3476-89.

Ravindra KC, Ho WE, Cheng C, et al (2015) Untargeted Proteomics and Systems-Based Mechanistic Investigation of Artesunate in Human Bronchial Epithelial Cells. Chem Res Toxicol. 28(10):1903-13.

Roberts RA, Ganey PE, Ju C, Kamendulis LM, Rusyn I, Klaunig JE (2007) Role of the Kupffer cell in mediating hepatic toxicity and carcinogenesis. Toxicol Sci 96:2–15.

Sarkar U, Rivera-Burgos D, Large EM, et al (2015) Metabolite Profiling and Pharmacokinetic Evaluation of Hydrocortisone in a Perfused Three-Dimensional Human Liver Bioreactor. Drug Metab Dispos 43(7):1091-9.

Schwarz M, Russell DW, Dietschy JM, Turley SD (2001) Alternate pathways of bile acid synthesis in the cholesterol 7alpha-hydroxylase knockout mouse are not upregulated by either cholesterol or cholestyramine feeding. J Lipid Res 42:1594–1603.

Skoutakis VA, Carter CA, Mickle TR, et al (1988) Review of diclofenac and evaluation of its place in therapy as a nonsteroidal antiinflammatory agent. Drug Intell Clin Pharm 22:850–859.

Szabo G and Petrasek J (2015) Inflammasome activation and fuction in liver disease. Nat Rev Gastroenterol Hepatol 12(7):387-400.

Tang W (2003) The metabolism of diclofenac--enzymology and toxicology perspectives. Curr Drug Metab 4:319–329.

Tsamandouras N, Kostrzewski T, Stokes CL, et al. (2016) Quantitative assesment of population variability in hepatic drug metabolism using a perfused three-dimensional human

liver microphysiological system. J Pharmacol Exp Ther. 2017 Jan;360(1):95-105. Epub 2016 Oct 19.

Wheeler SE, Clark AM, Taylor DP, Young CL, Pillai VC, Stolz DB, Venkataramanan R, Lauffenburger D, Griffith L, and Wells A (2014) Spontaneous dormancy of metastatic breast cancer cells in an all human liver microphysiologic system. Br J Cancer, 111(12):2342-50.

Zhang Y, Lee P, Liang S, et al (2015) Structural basis of non-steroidal anti-inflammatory drug diclofenac binding to human serum albumin. Chem Biol Drug Des. 2015 Nov;86(5):1178-84. doi: 10.1111/cbdd.12583. Epub 2015 May 28.

FOOTNOTES

FIGURE LEGENDS

Figure 1. Binding equilibrium between DCF and BSA: (A) Literature values of DCF-albumin equilibrium constants were used to predict a landscape of bound:free values for the interaction between DCF and BSA. Free DCF fraction was calculated with respect to BCA and DCF concentrations using the Scatchard equation (Dutta et al. 2006). (B) Free DCF concentrations were quantified in the cell culture medium with 1.25 mg/mL (20 µM) BSA, the concentration used for metabolism studies in this work. The experimental data agreed well with the literature-based predictions. Data correspond to mean values of two technical replicates.

Figure 2. DCF pharmacokinetics in the LiverChip™: (A) A 4.4 µM pharmacological dose of DCF and (B) a 440 µM suprapharmacological dose of DCF, were administered to separate wells of LiverChip™, in duplicate wells for each dose. Data for total DCF concentrations as a function of time are plotted for each dose (circles), and were used to generate a PK model taking into account both mixing and equilibrium binding to BSA (solid line). Each well was sampled twice in order to evaluate technical variation; individual samples–were assessed two times consecutively in positive ion mode using RP-UHPLC-TOF-MS.

Figure 3. Toxicity of DCF in LiverChip™ under basal and inflamed conditions: DCF was administered to primary human hepatocyte and Kupffer cell co-cultures in LiverChip™ and the response of the assayed using (A) WST-1, (B) LDH release, and (C) albumin secretion. Data correspond to mean values of two replicates for A and standard deviation

was based on n = 3 for B and C.

Figure 4. DCF biotrasformation: DCF metabolites from liver co-culture system were observed and included 4-hydroxy-DCF and 5-hydroxy DCF as major and minor phase I metabolites, respectively; and acylglucuronides of DCF, hydroxy-DCF as the major phase II metabolites. These metabolites were accounted for by CYP2C9, CYP2C8, and UGT2B7 metabolism in humans as well.

Figure 5. Bile acid synthesis: Bile acid synthesis and biotransformation in this LiverChip™ model may primarily stem from cholesterol metabolism by CYP7A1. Cholic, glycocholic, taurocholic, and glycochinodeoxycholic acids were detected by UHPLC-MS in the medium. A glycine-conjugated *e.g.,* GCA was the most abundant bile acid identified, and characterized as a biomarker in this co-culture system. Each well was sampled twice in order to evaluate technical variation.

Figure 6. **DCF induced toxicity and the effect of LPS**: (A) The MPS was treated with different doses of DCF (0, 44, 110, 220, and 440 μM) and analyzed by the LC-MS/MS method with d5-GCA as internal standard. GCA was found to be the most prevalent and sensitive small molecule markers, and may be a candidate early-indicator biomarker of liver toxicity. (2B) Untargeted metabolomics revealed changes in bile-acid production when the liver MPS was treated with LPS alone, DCF, and LPS + DCF only. Data correspond to mean values of two technical replicates.

Figure 7. Venn diagrams summarizing proteins identified in the liver bioreactor: (A-C) The overlap of proteins identified and compared between two different days with DCF treatment. Overview of location and function of proteins identified secreted proteins in hepatocyte medium by DCF treatment. (D) Classification of identified proteins based on relevant functional processes (gene ontology terms). (E) Cellular distribution of captured proteins.

Figure 8. **Venn diagrams summarizing selected APPs (only 19 shown in Table 1) identified in the liver bioreactor on Day 7**: (A-C) The overlap of proteins identified and compared between two different treatments. Proteins were identified with minimum of 2 peptides and 95% confidence.

Figure 9. LPS-induced inflammation profiles of secreted factors in co-cultures KC:Heps, 1:10 (A) Unsupervised hierarchical clustering of cytokines, chemokines, and growth factors assessed at 24 h (Day 7) in the presence or absence of 1 μg/mL LPS. Cultured medium of two replicates were sampled (rows) for 31 signaling factors (columns) detected above background levels. Secreted factor concentrations were mean-centered for comparison. This analysis confirmed elevated cytokine levels corresponding to LPS induction (red intensity values and dendrogram) and further identified a distinct profile associated with decreased levels of select analytes (blue intensity values and dendrogram) reproduced between replicates. (B) Secreted factors strongly elevated by LPS-induced inflammation ($15.8 \geq$ fold-change ≥ 6.2) due to LPS-induced inflammation. (C) Secreted factors mildly elevated by LPS-induced inflammation ($2.7 \geq$ fold-change ≥ 2.0). (D)

Secreted factors decreased by LPS-induced inflammation ($0.6 \geq$ fold-change ≥ 0.3). (E)

Fold-change presented for all 31 signaling factors detected. Full set of changes are shown in

Supplementary Figure S1.

Table 1. The ln2 quantitative iTRAQ values of APPs from Day 7. The drug and LPS treated samples were normalized to untreated sample (Control). The LPS and LPS along with drug treatment samples are normalized to LPS samples. As the values indicate the treatment of drug (DCF 440 µM) suppresses the synthesis of APPs.

	Drug/Control	LPS/Control	[LPS+Drug]/LPS	Proteins
1	1.4	3.0	-1.2	Transferrin
2	1.1	4.2	-1.9	Alpha-1-antitrypsin
3	1.0	4.2	-2.0	Alpha-1 antiproteinase
4	0.5	3.8	-1.3	Haptoglobin
5	3.4	3.9	0.1	Serum albumin
6	3.4	3.9	0.1	Hypothetical protein
7	-0.8	2.1	-1.0	Vitamin D-binding protein
8	1.2	3.8	-0.9	Ceruloplasmin
9	1.7	2.4	0.0	Liver carboxylesterase 1 isoform a
10	2.3	3.7	-1.2	Angiotensinogen
11	3.6	7.0	-1.3	Alpha-1-acid glycoprotein 1
12	-1.6	5.0	-1.5	Alpha-1-acid glycoprotein 2
13	0.3	1.5	-1.0	Alpha2-HS glycoprotein
14	-1.0	3.3	-2.0	Alpha 2 macroglobulin
15	2.7	5.0	-1.9	Retinol binding protein 4
16	1.8	5.1	-1.7	Complement component C3
17	1.2	1.3	-0.9	Transthyretin
18	1.5	2.8	-0.5	Leucine-rich alpha-2-glycoprotein
19	2.3	-1.7	8.5	Amyloid beta A4 protein isoform b

Table 2. Levels of GCA detected after 48 h. DCF concentrations of 440 μM and 110 μM reduced the relative amounts of bile acids at earliest time point. At Day 5 cholic acid, taurocholic acid, glycochenodeoxycholic acids and GCA were detected as the major bile acids. GCA was the most abundant bile acid identified in this 3D liver culture. Peak intensity (EIC%) relative values were for guidance only. They do not represent absolute amounts present in these experiments. Bile acids peak areas were compared to GCA peak area and found to be lower. GCA production was relatively stable over several days (data not shown).

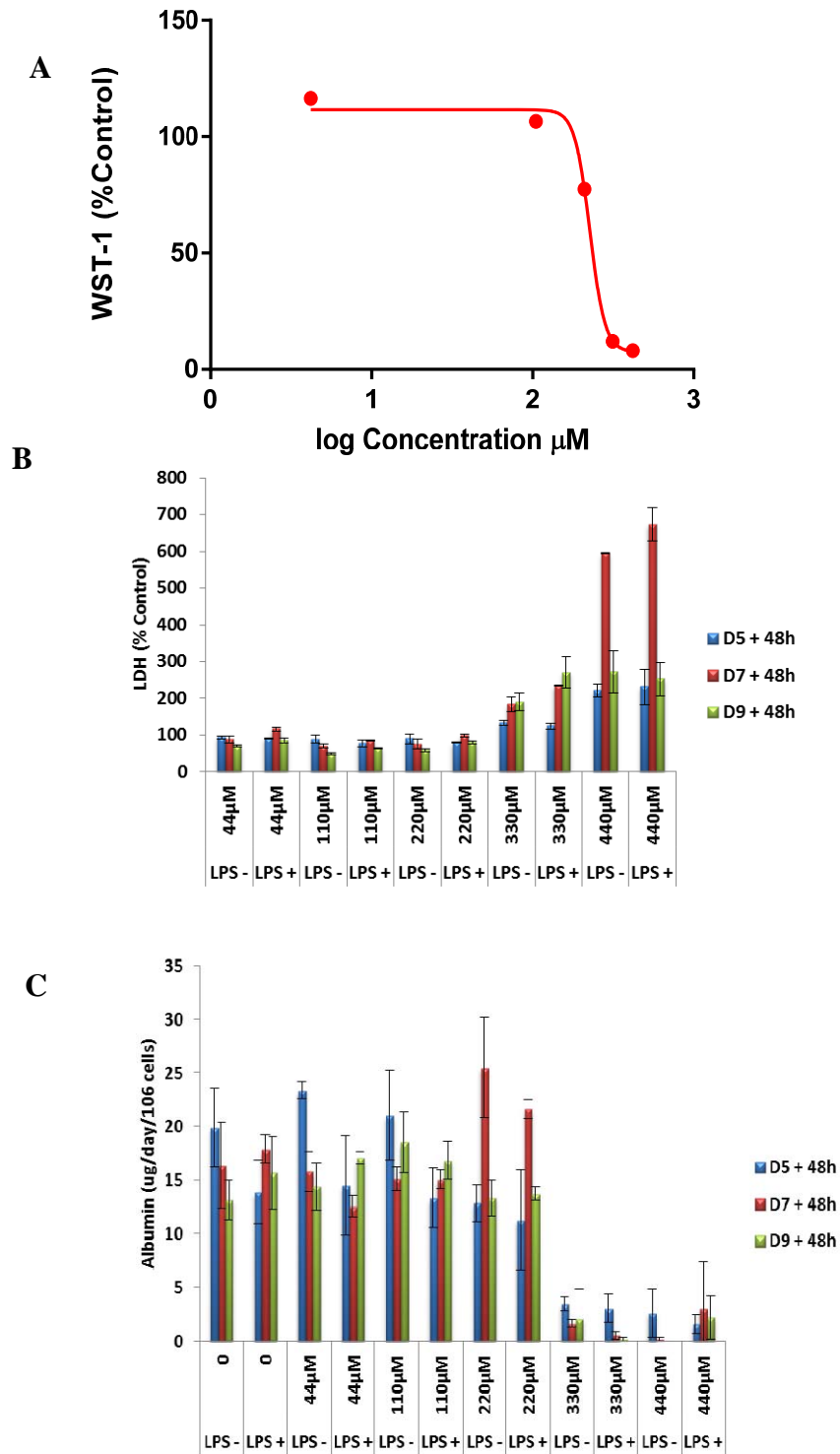| Bile acids; (ratio provided compared to GCA signal)	% levels of detected bile acids after 48 h		
	DCF; 0 μM	DCF; 110 μM	DCF; 440 μM
Cholic acid; 1	100%	66%	12%
Taurocholic acid; 2	100%	77%	10%
Glycocholic acid (GCA); 100	100%	57%	2%
Glycochenodeoxycholic acid; 10	100%	50%	15%
Glycochenodeoxycholic acid 3-glucuronide; 0.2	100%	69%	14%

FIGURES

Figure 1.
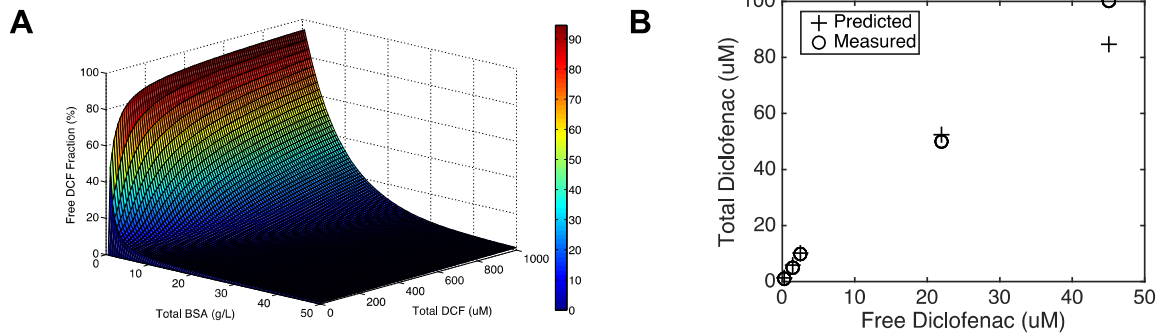
Figure 2.
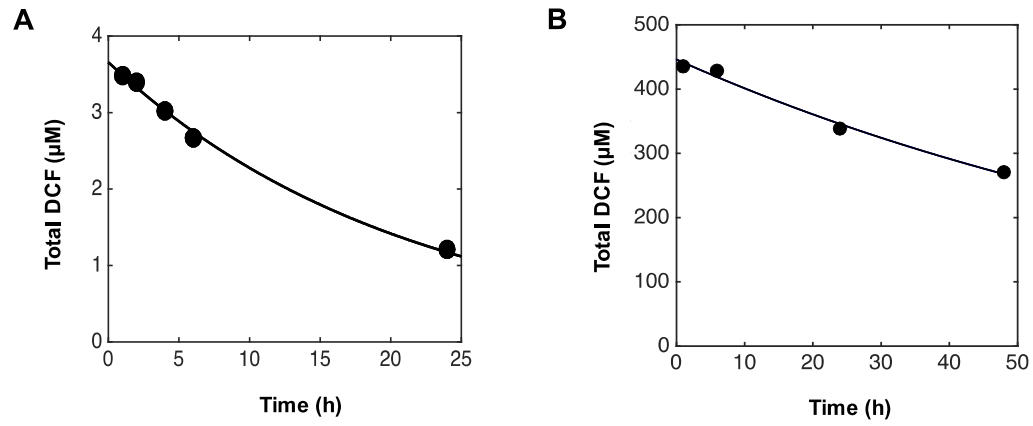
Figure 3.

Figure 4.
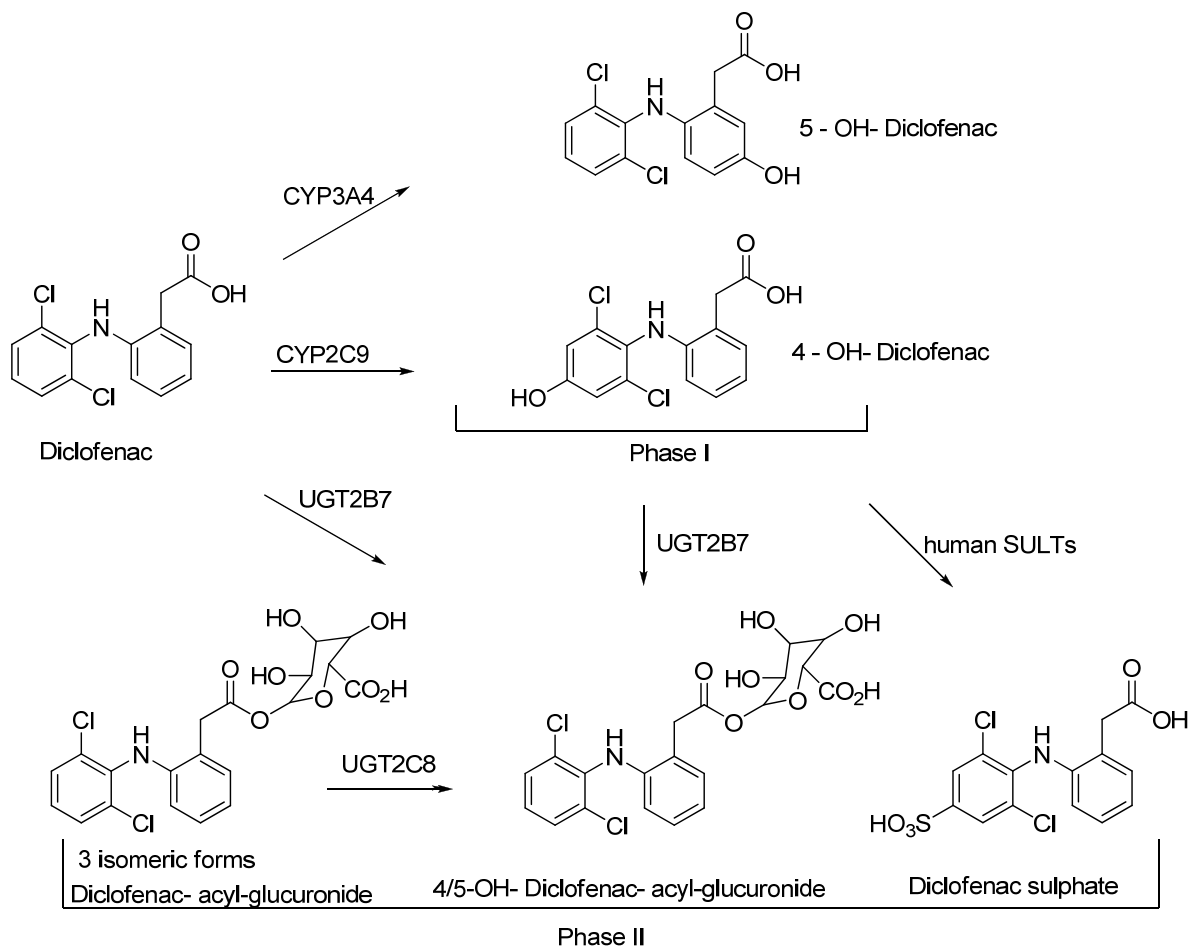
Figure 5.
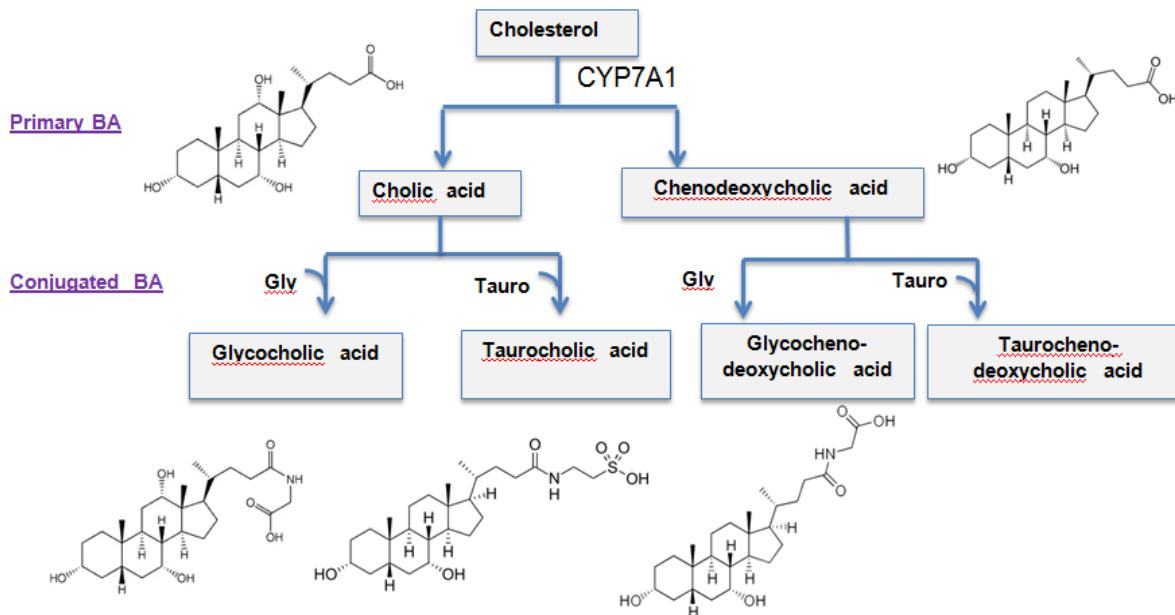
Figure 6.
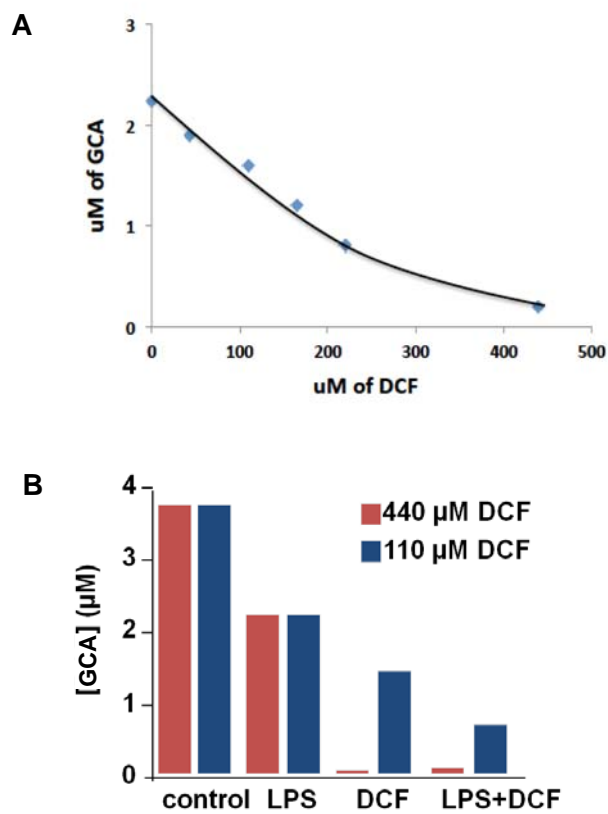
Figure 7.

Figure 8.

Figure 9.